International Journal of Geometric Methods in Modern Physics
Vol. 18, No. 10 (2021) 2150154 (21 pages)

DOI: 10.1142/S0219887821501541

Quasinormal modes of *dS* and *AdS* black holes: Feedforward neural network method

Ali Övgün* and İzzet Sakallı†

Physics Department, Eastern Mediterranean University
Famagusta, 99628 North Cyprus, via Mersin 10, Turkey
**ali.ovgun@emu.edu.tr*
†*izzet.sakalli@emu.edu.tr*

Halil Mutuk‡

Physics Department, Faculty of Arts and Sciences
Ondokuz Mayis University, 55139 Samsun, Turkey
hmutuk@omu.edu.tr

Received 26 October 2020
Revised 13 May 2021
Accepted 17 May 2021
Published 11 June 2021

In this paper, we show how the quasinormal modes (QNMs) arise from the perturbations of massive scalar fields propagating in the curved background by using the artificial neural networks. To this end, we architect a special algorithm for the feedforward neural network method (FNNM) to compute the QNMs complying with the certain types of boundary conditions. To test the reliability of the method, we consider two black hole spacetimes whose QNMs are well known: $4D$ pure de Sitter (dS) and five-dimensional Schwarzschild anti-de Sitter (AdS) black holes. Using the FNNM, the QNMs of are computed numerically. It is shown that the obtained QNMs via the FNNM are in good agreement with their former QNM results resulting from the other methods. Therefore, our method of finding the QNMs can be used for other curved spacetimes that obey the same boundary conditions.

Keywords: Quasinormal modes; feedforward neural network; de Sitter; anti-de Sitter; black hole.

Mathematics Subject Classification 2020: 83C35, 83C57, 68T01, 68T20

1. Introduction

QNMs are single frequency modes dominating the time evolution of perturbations of systems which are subject to damping, either by internal dissipation or by radiating away energy. Due to the damping, the frequency of a QNM must be complex, its imaginary part being inversely proportional to the typical damping time. Recall

‡Corresponding author.

that, in general relativity, damping occurs even without friction, since energy may be radiated away towards infinity by gravitational waves [1,2]. Thus, they could lead to the *direct* identification of the existence of the BH through gravitational wave observation, which might be realized in the near future. QNMs, which are believed to be characteristic sounds of perturbed black hole (BH) spacetimes, have been investigated for a long time and their physical properties have been presented in various studies (see for example [3–28]). It is worth noting that similar to the BH geometries, QNMs can also arise from other spacetimes including the wormholes [33–66].

Since the discovery of the *AdS/CFT* correspondence [68], QNMs of *AdS* spacetimes have become very attractive over the past two decades. Besides, it is suggested that QNMs of *AdS* BHs are related with the double conformal field theory (CFT) [69–74]. Since the QNMs govern the deterioration time of a perturbed BH, within the bulk, configuration, they should be associated with the *AdS/CFT* duality in order to return the boundary of Yang–Mills theory to the thermal equilibrium. The numerical computations of QNMs for *AdS* BHs in arbitrary dimensions were served in [69]. Then, Govindarajan and Suneeta [75] computed the QNMs of the $5D$ *AdS*-Schwarzschild BH by using the superpotential approach. Moreover, in the framework of scalar perturbation spectra, it was known that there exists a relation between (bulk) *dS* spacetime and the corresponding CFT at the boundaries (*past* I^- and *future* I^+) [76], which provides a quantitative support for the dS/CFT correspondence. The relation between the QNMs and surface gravity (κ) of the cosmological horizon was thoroughly discussed in [77]. Unlike the massless minimally coupled scalar field, it was shown that for a massive scalar field there exists QNMs in the pure *dS* spacetimes. Even the obtained QNMs of pure *dS* spaces are analytical frequencies [78].

New derivations of the QNMs for the curved spacetimes have always attracted a great attention. This challenge stems from the fact that it is difficult to solve the wave equations of the considered fields, analytically. Therefore, many numerical techniques have been developed in order to solve those type of equations. In recent decades, the artificial neural networks (ANNs) [81] have been employed for finding solutions of differential equations which appeared in the different physical systems. As is well known, FNNM was the first and simplest type of ANN devised. In this network, the information moves in only one direction forward from the input nodes, through the hidden nodes (if any) and to the output nodes. There are no cycles or loops in the network [82]. FNNM or such connectionist systems compute the systems uncertainly inspired by the biological nervous (neural) systems that constitute animal brains and also there are many applications in general relativity and cosmology [83–94]. Some of the advantages of using FNNM in solving the differential equations are listed as follows [95–98]:

- Solution in the domain/field of integration is continuous [99],
- Computing complexity does not increase significantly with increasing number of sampling points and dimensions,

- Rounding-off error propagation does not alter the ANN solution, which happens in standard numerical methods

In this paper, we separately compute the QNMs for the four-dimensional pure *dS* space [78, 100] and the $5D$ *AdS*-Schwarzschild BH [101] by using the FNNM within the framework of *supervised learning* (see for instance [102] and references therein). In fact, the supervised learning algorithm analyzes some training (educational) data and generates an inference (or the so-called *trial*) function that can be used to achieve new results. This requires that the learning algorithm should be reasonably generalized from the educational data to situations that are not visible. It was also shown in [103] that the accuracy of the results obtained from the neural network surpasses the accuracy of other machine learning algorithms like SVM (*support vector machines*) and RF (*random forest*). While performing the computations, we consider the massive scalar field perturbations of the associated spacetimes. Finally, we compare the QNM values obtained with the FNNM with the results found from the other methods.

This paper is organized as follows. In Sec. 2, we briefly review the QNMs of the $4D$ pure *dS* and the $5D$ *AdS*-Schwarzschild BH. In Sec. 3, we describe the FNNM and show how one can compute the QNMs of those *dS/AdS* spacetimes. Then, we present and compare our results with the known ones. Finally, we conclude the paper with discussions in Sec. 4. We use natural units with $G = \hbar = c = 1$.

2. QNMs of Pure *dS* and *AdS*-Schwarzschild BHs

In this section, we shall make a brief overview of the QNMs of the pure *dS* and *AdS* spacetimes, which were obtained by the methods of analytical and super potential approach, respectively. We first consider the pure *dS* spacetime, which is given by the following $4D$ line-element [100]:

$$ds^2 = -f(r)dt^2 + f^{-1}(r)dr^2 + r^2 d\Omega_2^2, \tag{1}$$

where $f(r) = 1 - (\frac{r}{l})^2$ in which l denotes the minimal radius of *dS* space. Furthermore, $r^2 d\Omega_2^2$ is the metric on the $2D$ sphere of radius r. For the massive scalar field Φ perturbations, one should consider the Klein–Gordon equation:

$$\Phi^{;\nu}{}_{;\nu} = m^2 \Phi, \tag{2}$$

which can be separated by

$$\Phi = \frac{\Psi^{dS}(r)}{r} e^{-i\omega t} Y_\ell(\Omega_2). \tag{3}$$

Here, $Y_\ell(\Omega_2)$ is nothing but the spherical harmonics, which corresponds to the eigenfunction of two-dimensional Laplace–Beltrami operator ∇_2^2 having the eigenvalue $-\ell(\ell+1)$. Recalling definition of the tortoise coordinate, we get

$$r_* = \int \frac{dr}{f(r)} = l \tanh^{-1}\left(\frac{r}{l}\right). \tag{4}$$

Thus, one obtains the radial equation in the form of $1D$ Schrödinger-like wave equation

$$-\frac{d^2\Psi^{dS}}{dr_*{}^2}+\left[V_0^{dS}(r)-\omega^2\right]\Psi^{dS}=0, \tag{5}$$

where the effective potential reads

$$V_0^{dS}(r)=\frac{1}{l^2}\left[\frac{\ell(\ell+1)}{\sinh^2(r_*/l)}-\frac{2-m^2l^2}{\cosh^2(r_*/l)}\right], \tag{6}$$

Since $\ell(\ell+1)\geq 0$, the effective potential (6) diverges ($\to\infty$) at the singularity ($r=0$) and vanishes at the cosmological horizon (r_h). For this reason, QNMs obey the following boundary conditions: purely outgoing wave at the cosmological horizon and vanish at the singularity [78]. Meanwhile, at this stage, it is worth noting the late-time tails [79] cannot be addressed by merely studying Eq. (5) (the reader can refer to [80]). After deriving the exact analytical solution of the radial equation in terms of the hypergeometric function and in the sequel imposing the boundary conditions, it was found that to have non-zero QNMs there is a lowest bound: $m>\frac{3}{2l}$ on the mass of scalar field Φ. The resulting QNM sets were given by [78] as follows:

$$\omega_I=\pm\frac{1}{l}\left[m^2l^2-\frac{9}{4}\right]^{\frac{1}{2}}-\frac{i}{l}\left(2n+\ell+\frac{3}{2}\right) \tag{7}$$

$$\text{or}\quad \omega_{II}=\pm\frac{1}{l}\left[m^2l^2-\frac{9}{4}\right]^{\frac{1}{2}}-\frac{i}{l}\left(2n-\ell+\frac{1}{2}\right). \tag{8}$$

The difference in sets is due to the poles of the gamma functions that help us to sort out the waves on the horizon only as outgoing waves. Without loss of generality, when comparing the above results with the FNN method to be applied, we will consider the first set as

$$\omega=\frac{1}{l}\left(m^2l^2-\frac{9}{4}\right)^{\frac{1}{2}}-\frac{i}{l}\left(2n+\ell+\frac{3}{2}\right). \tag{9}$$

On the other hand, $5D$ *AdS*-Schwarzschild BH is given by [101]

$$ds^2=-N(r)dt^2+N^{-1}(r)dr^2+r^2d\Omega_3^2, \tag{10}$$

where

$$N(r)=1+\left(\frac{r}{l}\right)^2-\left(\frac{r_0}{r}\right)^2. \tag{11}$$

The relationship between r_0 and the BH mass M is given by

$$M=\frac{3A_3r_0^2}{16\pi G_5}, \tag{12}$$

where A_3 denotes the area of a unit $3D$-sphere described by $d\Omega_3^2$. Using the ansatz for the scalar field

$$\Phi=r^{-3/2}\Psi^{AdS}(r)\exp(i\omega t), \tag{13}$$

the massless Klein–Gordon equation of metric (10) yields the following one-dimensional Schrödinger-like wave equation:

$$-\frac{d^2\Psi^{AdS}}{{dr_*}^2}+\left[V_0^{AdS}(r)-\omega^2\right]\Psi^{AdS}=0, \tag{14}$$

where $dr_*=\frac{dr}{N(r)}$ and the effective potential becomes (for simplicity, the authors of [101] had taken $l=1$ and we will also stick to their choice in our computations in order to make a consistent comparison):

$$V_0^{AdS}(r)=N(r)\left(\frac{15}{4}+\frac{3}{4r^2}+\frac{9r_0^2}{4r^4}\right). \tag{15}$$

It is clear from Eq. (15) that $V_0^{AdS}\to\infty$ at spatial infinity ($r=\infty$) and vanishes at the horizon $\left[r=r_+\to N(r_+)=0\right]$. For this reason, QNMs of obey the following boundary condition: purely ingoing wave at the horizon and vanish at the spatial infinity. Since the fundamental QNMs of the Schwarzschild BH are closely approximated by the QNMs of the Pöschl–Teller potential, in the spirit of the Pöschl–Teller method for asymptotically flat BHs, the QNMs for the *AdS*-Schwarzschild BH in $5D$, using a superpotential approach, were obtained and served in [101, Table I]. In general, for the asymptotically flat BHs, the QNMs correspond to solutions of the wave equations with the physical boundary conditions of purely outgoing waves at spatial infinity and purely ingoing waves crossing the event horizon [104, 105]. However, for the *AdS*-Schwarzschild BH, QNMs should admit wave functions that must be purely ingoing wave at the horizon and no outgoing wave at spatial infinity. Namely, at the asymptotic regions, all QNMs of the *AdS* BH are required to terminate. Thus, as being highlighted in [101], any numerical calculation of QNMs is very *artful* due to the nature of the boundary conditions. During the numerical computations, one must ensure to have pure ingoing wave near the horizon, which could be contaminated by an outgoing wave and the correct *asymptotic* behavior of the wave function that fades away as $r\to\infty$. In the superpotential method [101], as in the continued fraction method [106] which is suitable for the asymptotically flat BHs, a particular ansatz for the wave function was introduced to meet all boundary conditions. Similarly, in the FNNM method, a trial solution or ansatz that meets the boundary requirements will have to be sought.

3. FNNM

A complicated problem in science can be solved analytically or numerically in terms of known methods. In most of the cases, an analytical solution to the associated differential equation may not be obtained easily and it is usually cumbersome. Various types of numerical methods have been developed to solve such transcendental differential equations such as shooting, Euler, Runge–Kutta, finite difference, finite element, finite volume, Adomian decomposition, asymptotic iteration, variational iteration, and perturbation methods. All these methods have both advantages and shortcomings. Although they provide good approximate solutions, these meth-

ods require discretization of the domain of the problem. Most of these numerical methods give solutions over discrete points and the solution between these points needs to be interpolated. Besides, these methods are in general iterative such that one should fix the step-size before solving the considered problem. The advantages of employing the ANNs (and whence the FNNM) can be listed as follows [95, 96]:

- Solving differential equation by neural network framework presents solution with a very good generalization properties.
- The method is general and can be applied to the systems defined on either orthogonal box boundaries or on irregular arbitrary shaped boundaries.
- The ANN method can be implemented on parallel architectures which can be used in more complex problems.
- The ANN method spends negligible computing time and memory.
- If the model has free parameters, they can be treated as variables in the ANN method.

Most of the problems which cannot be solved analytically are turned into an mathematical optimization problem in which a numerical solution is sought. This optimization can be done in some techniques. Since the problem is considered in a specific region (i.e. the convergence problem), the transition between local and global solutions require intensive processing. In this perspective, the ANNs have broad usage field and they are powerful tools for performing a mathematical modeling.

An ANN can be defined as parallel information processor in which a number of neurons are distributed as operating units. This information processing system can take many input from outside, combines them via mostly nonlinear operations and produce the output. Nowadays, ANN is one of the popular topics of machine learning paradigm. They have a wide range of usage from pattern recognition to financial forecast including classification, decoding speech, etc. ANNs are typically composed of layers. These layers are made of interconnected neurons (perceptrons in modern computers). A neuron is the main processing element in the ANN. Because, neurons have activation functions which translate input signals to output signals. Problem solving process in the ANN occurs by acquiring knowledge. This mechanism is maintained by learning methods and information is stored within 'interneuron connections' strength which can be calculated by some numerical values called weights [107, 108].

The detailed computational steps of the working principle of an artificial neuron in a neural network can be seen in Fig. 1.

A neuron N_i receives inputs n which belong to $S = \{x_j \,|\, j = 1, 2, \ldots, n\}$. Each input is multiplied by a weight factor w_{ij} for $j = 1, 2, \ldots, n$ before entering to the neuron N_i. In general, this neuron has a bias term w_0 and a critical value θ_k. To

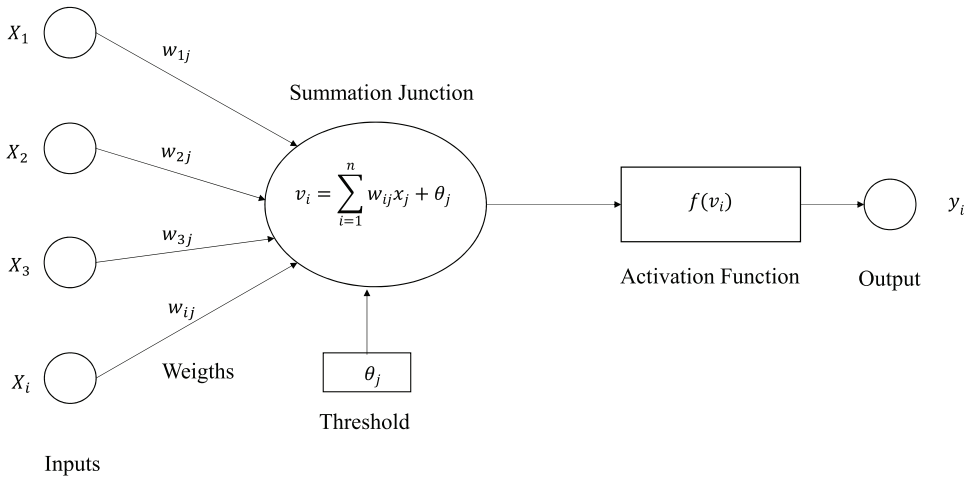

Fig. 1. Basic model of multi-inputs one-output neuron.

produce the output signal, this critical value must be reached and/or exceeded. The input of the ith neuron N_i in the input layer can be written as

$$v_i = w_0 + \sum_{k=1}^{n} w_{ik}x_k. \tag{16}$$

The neurons in the input layer can work only if the signal reaches/exceeds the critical value which can be defined as the neuron's working condition as

$$w_0 + \sum_{k=1}^{n} w_{ik}x_k \geq \theta. \tag{17}$$

All the input signals are multiplied by their synaptic weights and added together. This compose "net" input to the neuron:

$$\text{net} = \sum_{k=1} w_{ik}x_k + \theta, \tag{18}$$

where θ is the threshold (i.e. critical) value. The output signal of ith neuron N_i can be functionalized as

$$O_i = \left(w_0 + \sum_{k=1}^{n} w_{ik}x_k \right). \tag{19}$$

An activation function acts on the produced weighted signal which is denoted as $\sigma(s)$. The output signal y can be obtained by mapping this activation function as

$$y = \sigma(\text{net}) = \sigma \left(\sum_{j=1}^{n} w_{ij}x_j + \theta \right), \tag{20}$$

where σ denotes the neuron activation function. This output function is suggested together with a critical function. In this work, we will use a sigmoid activation

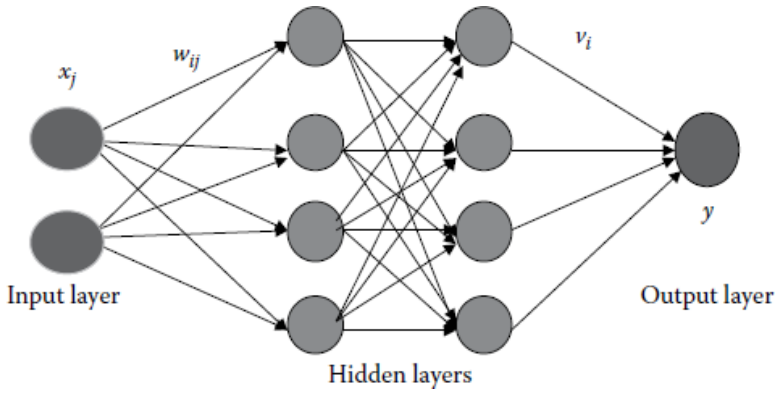

Fig. 2. A sample architecture of an ANN.

function

$$\sigma(x) = \frac{1}{1+e^{-x}} \tag{21}$$

which is a traditional one for obtaining solutions in nonlinear problems.

A diagram of a multilayer ANN is given in Fig. 2.

The information are given to the input layer, which sends the information to the hidden layer, if any exists. The processing of inputs is being done at this stage via a system of weighted connections. The hidden layers send the information to the output layer and an answer is given to the outside world. In Fig. 2, x_j are input nodes, ω_{ij} are weights from input to the hidden layer (or layers if exist), and ν_i are synaptic weights from hidden to the output layer y which is the output node [107]. The neurons in the same layer have no connection among themselves. If there is more than one hidden layer, the architecture is known as deep neural network which is out of the scope of this work.

In this work, we used an architecture which consists of one input layer, one hidden layer and one output layer. This ANN architecture can be seen in Fig. 3. Neurons are arranged into distinct layers with each layer receiving input from the previous layer and outputting to the next layer. In this manner, neurons (processing elements) in a layer receive input from the previous layer and send (feed) their output to the next layer.

Initial weights from the input layer to the hidden layer (w_j) and from the hidden layer to the output layer (v_j) are taken as arbitrary (random). The number of nodes in the hidden layer is determined by the trial-and-error method.

3.1. *Implementation of ANN on quantum systems*

The framework for FNNM to obtain solutions of eigenvalue equations was developed in [109]. A differential equation can be written as

$$H\Psi(r) = \wp(r), \quad \text{in } \mathcal{D} \tag{22}$$

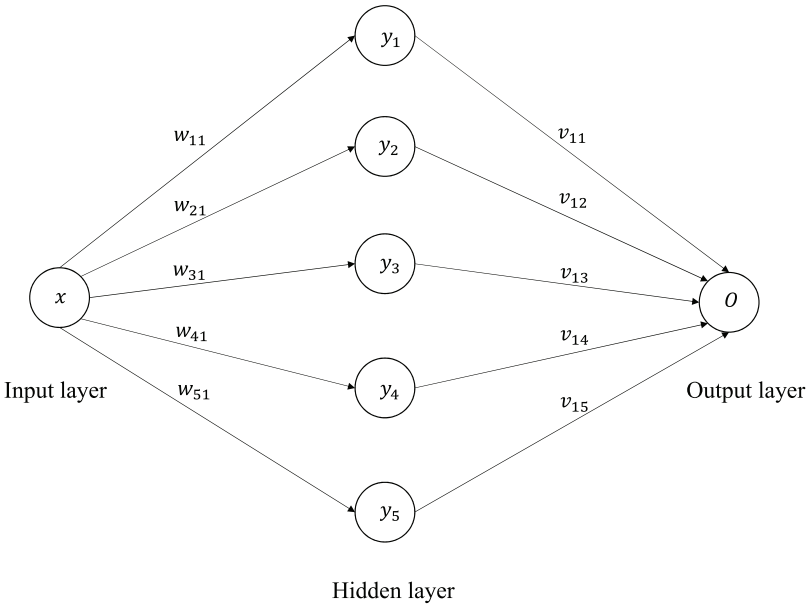

Fig. 3. ANN architecture of this work.

with

$$\Psi(r) = 0 \quad \text{on } \partial\mathcal{D}. \tag{23}$$

Here, H is a linear operator, $\wp(r)$ is a *known* function and $\partial\mathcal{D}$ is the boundary of $\mathcal{D}$. In order to solve Eq. (22), a trial function

$$\Psi_t(\mathbf{r}) = A(\mathbf{r}) + B(\mathbf{r}, \boldsymbol{\lambda})N(\mathbf{r}, \mathbf{p}) \tag{24}$$

can be used. This function proceeds to a neural network with a vector parameter $\mathbf{p}$ and undetermined parameter $\boldsymbol{\lambda}$ which is going to be adjusted later. $N(\mathbf{r}, \mathbf{p})$ is a single-output feed forward neural network with parameters $\mathbf{p}$ and n input units fed with the input vector $\mathbf{r}$. The functions A and B will be determined with respect to appropriate $\Psi_t(\mathbf{r})$ which satisfies the boundary conditions.

To solve Eq. (22), the *collocation* method [110] can be used. The idea behind the collocation method is to choose a finite-dimensional space of trial solution functions and a number of points in the domain of the problem, and to select that trial solution which satisfies the given equation at the collocation points. This procedure discrete the domain into a set of $\mathbf{r}_i$. To this end, one can get a minimization problem as follows:

$$\min_{p,\lambda} \sum_i [H\Psi_t(r_i) - \wp(r_i)]^2. \tag{25}$$

To have the Schrödinger equation, one can recast Eq. (22) in an eigenvalue equation:

$$H\Psi(r) = \omega^2\Psi(r) \tag{26}$$

with the boundary condition $\Psi(r=0)=0$. Before obtaining QNMS via FFNM, an important notice should be done. In this work, we assume the foreknown definition of the QNMs that these modes are purely outgoing waves at the event horizon of black hole r_h, where is the boundary defining the region of space around a black hole from which nothing (not even light) can escape and vanish at $r=0$ [78]. These boundary conditions are determined by the behavior of the effective potential: recall Eqs. (6) and (15), which are obtained for dS and AdS spacetimes, respectively. Thus, the trial solution becomes

$$\Psi_t(r) = B(\mathbf{r},\boldsymbol{\lambda})N(\mathbf{r},\mathbf{p}), \tag{27}$$

where $B(\mathbf{r},\boldsymbol{\lambda})=0$ at boundaries for a range of λ values. Employing the discretization for the domain of the problem together with the collocation method, a minimization problem can be obtained with respect to the $\mathbf{p}$ and $\boldsymbol{\lambda}$:

$$E(\mathbf{p},\boldsymbol{\lambda}) = \frac{\sum_i \left[H\Psi_t(r_i,\mathbf{p},\boldsymbol{\lambda}) - \omega^2\Psi_t(r_i,\mathbf{p},\boldsymbol{\lambda})\right]^2}{\int |\Psi_t|^2 d\mathbf{r}}, \tag{28}$$

where E represents the error function. Furthermore, ω^2 is obtained as follows:

$$\omega^2 = \frac{\int \Psi_t^* H\Psi_t d\mathbf{r}}{\int |\Psi_t|^2 d\mathbf{r}}. \tag{29}$$

Thus, the energy eigenvalues or the QNMs are given by

$$\omega = \left(\frac{1}{\int |\Psi_t|^2 d\mathbf{r}}\left[\int_{r_1}^{r_2}\left(\frac{d\Psi_t}{dr}\right)^2 dr + \int_{r_1}^{r_2} V_0(r)\Psi_t^2(r)dr\right]\right)^{\frac{1}{2}}, \tag{30}$$

where r_2 represents the location where the scalar field becomes pure plane wave (ingoing/outgoing) and r_1 indicates the radial position where the effective potential diverges and whence causes the waves to be completely damped (i.e. $\Psi_t = 0$). Therefore, while $r_1=0$ and $r_2=r_h$ for the pure dS BH, in the AdS BH we take $r_1=\infty$ and $r_2=r_+$. V_0 corresponds to the effective potential of the spacetime taken into account.

The parameter $\mathbf{p}$ is nothing but the weights and biases of the ANN. Although the multi-layer sensor (MLP) has many hidden layers, here we use a simple model of a single hidden layer MLPs. In this study, we also consider a multilayer perception with n input units, one hidden layer having m units, and an output. Given an input vector

$$\mathbf{r} = (r_1,\ldots,r_n), \tag{31}$$

the output of the neural network can be written as

$$N = \sum_{i=1}^{m} \nu_i \sigma(z_i), \tag{32}$$

where

$$z_i = \sum_{j=1}^{n} \gamma_{ij} r_j + u_i. \tag{33}$$

Here, γ_{ij} are the weights from input unit j to the hidden unit i, ν_i is the weight from hidden unit i to the output unit, u_i represents the bias of hidden unit i, and $\sigma(z)$ is the sigmoid function, which is given in Eq. (21). The derivatives of the ANN output can be written as

$$\frac{\partial^k N}{\partial r_j^k} = \sum_{i=1}^{m} \nu_i \gamma_{ij}^k \sigma_i^{(k)}, \tag{34}$$

where $\sigma_i = \sigma(z_i)$ and $\sigma^{(k)}$ is the k^{th} order derivative of the activation (sigmoid) function.

One can parametrize the solution trial function as

$$\phi_t(r) = e^{-\beta r^2} N(r, \mathbf{u}, \mathbf{w}, \mathbf{v}), \quad \beta > 0, \tag{35}$$

where N denotes a feedforward neural network with one hidden layer and m sigmoid hidden units

$$N(r, \mathbf{u}, \mathbf{w}, \mathbf{v}) = \sum_{j=1}^{\bar{m}} \nu_j \sigma(\omega_j r + u_j). \tag{36}$$

The minimization problem turns out to be as

$$\frac{\sum_i \left[H\phi_t(r_i) - \omega^2 \phi_t(r_i)\right]^2}{\int |\phi_t(r)|^2 dr}. \tag{37}$$

Solving this equation is equivalence to solving Schrödinger equation. The minimization problem can be solved via collocation method. In this method, one chooses a finite-dimensional space of solution trial function which is supposed to solve given differential equation with a number of points in the domain.

In order to obtain the desired result, ANN needs to learn. Solving a differential equation within ANN method requires training of the ANN. This learning process can be done in different ways. In this work, we used error back-propagation learning algorithm. This learning algorithm is one of the most common used learning rules and it is valid for continuous activation function such as sigmoid function Eq. (21). By taking the partial derivative of the error function according to each weight, we can monitor the flow of the error direction in the network. The steps for the learning algorithm of back-propagation are as follows [107, 108]:

(1) Set the weights w and v from the hidden to the output layer. Choose the learning parameter in the range $(0, 1)$, and error $E_{\max}$. At the first step, error is taken to be zero.
(2) Train the network.
(3) Find the output of error function.

(4) Calculate the error signal terms by output and hidden layers, respectively.
(5) Calculate the error components for gradient vectors.
(6) Check if weights are adjusted appropriately.
(7) If $E = E_{\max}$, then cease the training. If not, proceed to step 2 by setting $E \to 0$ and initiate the new training.

The crucial point for the training process is taking the eigenvalue (error function) E as zero and train the neural network with equidistant points in the given interval of the problem. It is expected that this process yields energy function (eigenvalue) to be zero or at least converge to zero. If the convergence is not obtained, then the eigenvalue is wrong. If this happens, eigenvalue should be changed in a proper way and the training process should be restarted. It should be keep doing this process until the energy (error) function converges to zero.

It should also be noted that the method for solving differential equations with ANNs does not depend on the training method: The choice of training method only affects the speed of the training procedure.

Table 1. Comparison of FNNM QNMs with numerical QNMs obtained, via the superpotential approach method, for the *AdS* spacetime [101] (for $l = 0.001$ *case*). Percentual error (PE) rates are given.

(n, ℓ)	This work	[78]	PE (%)
$(0, 0)$	$0. - 3017i$	$0. - 3000i$	0.56
$(0, 1)$	$0. - 3994i$	$0. - 4000i$	0.15
$(1, 1)$	$0. - 6012i$	$0. - 6000i$	0.2
$(0, 2)$	$0. - 5024i$	$0. - 5000i$	0.48
$(1, 2)$	$0. - 7019i$	$0. - 7000i$	0.27
$(2, 2)$	$0. - 9037i$	$0. - 9000i$	0.41
$(0, 3)$	$0. - 6072i$	$0. - 6000i$	1.2
$(1, 3)$	$0. - 8056i$	$0. - 8000i$	0.7
$(2, 3)$	$0. - 10094i$	$0. - 10000i$	0.94
$(3, 3)$	$0. - 12103i$	$0. - 12000i$	0.85

Table 2. Comparison of FNNM QNMs with analytical QNMs obtained for the pure *dS* spacetime [78]. PE rates are also shown.

Radius, $r+$	This work	[101]	PE (%) real	PE (%) imaginary
1	$0.6960 + 1.4629i$	$0.6948 + 1.4648i$	0.17	0.12
2	$1.0774 + 1.9849i$	$1.0713 + 1.9817i$	0.56	0.16
5	$2.4407 + 4.2689i$	$2.4462 + 4.2642i$	0.22	0.11
10	$4.8205 + 8.3285i$	$4.8249 + 8.3279i$	0.09	0.07
50	$24.0731 + 41.3784i$	$24.0159 + 41.3183i$	0.23	0.04
100	$48.0376 + 82.6577i$	$48.0251 + 82.6165i$	0.02	0.01
150	$72.0373 + 123.9374i$	$72.0358 + 123.9190i$	0.06	0.01
500	$240.1166 + 413.0576i$	$240.1150 + 413.0500i$	0.01	0.01
750	$360.1145 + 619.5867i$	$360.1720 + 619.5740$	0.01	0.01
1000	$480.2143 + 826.0761$	$480.2290 + 826.0980$	0.03	0.02

3.2. *QNMs of Pure dS and AdS-Schwarzschild BHs via FNNM*

To derive the QNMS of the pure *dS* and *AdS*-Schwarzschild BHs, we first consider Eqs. (6) and (15), respectively, in Eq. (30), then compute the QNMs with the expression seen in Eq. (30). To this end, we employ the Gauss–Legendre rule [109] and use 200 equidistant points in the interval $0 < r < 10$ with $\bar{m} = 10$. In Tables 1 and 2, we represent our findings, which are the numerical values (via the FNNM within the context of supervised learning) of the QNMs of the pure *dS* and *AdS* spacetimes. It can be seen from those tables that FNNM satisfactorily re-derives the well-accepted QNMs' results obtained from the other methods [78, 101]. Thus, we have managed to introduce a new and effective method to the literature for computing the QNMs.

As mentioned above, the main advantage of using ANN is to solve the Schrödinger equation. However, the computational complexity while using the ANN does not increase considerably with the number of sampling points and with the number of dimensions in the problem. Depending on the learning algorithm, the running CPU time can be lowered significantly to obtain the solution. On the other hand, we shall not perform any CPU time comparison in this study, because it is irrelevant with the scope of the paper.

4. Conclusions

In this study, we have prescribed a new method, FNNM, to study the QNMs of BHs that posses particular boundary conditions as being described in Sec. 2. To test the method, we have considered the $4D$ pure *dS* and $5D$ *AdS*-Schwarzschild BHs. Scalar field perturbations have been treated as oscillations in the frequency domain of those static and symmetric backgrounds. In each geometry, the perturbed scalar fields are reduced to $1D$ Schrödinger-like wave equations with the associated effective potential. Imposing the required boundary conditions given in [78, 101], we have demonstrated how the FNNM derives the QNMs: the resulting formula is Eq. (30). After comparing our findings with the previous results obtained by the analytical method [78] and the superpotential approach (numerical) method [101], it is seen that the all results are in good agreement with each other. Therefore, FNNM is not only an alternative but an effective way for computing the QNMs that are important for the stability of a BH and the late-time behavior of radiation from gravitationally collapsing configurations. On the other hand, one may ask that how about for neural network solutions to the completely unknown problems. For such a case, the architecture and training processes must be different than the FNNM that we employed here. In fact, such an architecture is more about interacting with "*experimental data*" like "a *direct adaptive neural network method*" [111] in which the system took into account was described by an unknown NARMA model [111] and the FNNM was considered to learn the system. By taking the FNNM as a neural model, the control signals can easily be obtained by minimizing momentary difference or cumulative differences between a set point and the output

of the FNNM. Since the training algorithm can ensure that the output of the FNNM approaches to the real system, then it can be demonstrated how the obtained control signals make the real system output as being close to the set point [112]. However, such an algorithm cannot be established without having experimental data on the BHs that we work with. Namely, with the development of technology related to the BHs, it might be possible to construct such a neural network algorithm.

Further work to determine the QNMs of rotating and/or higher/lower dimensional *dS/AdS* spacetimes via the FNNM could therefore be interesting. Besides, we aim to extend our analysis to the Dirac (e.g. the reader is referred to this recent study [113]) and Maxwell equations that are formulated in the Newman–Penrose formalism [114–116] in the near future. Moreover, starting from Kerr BH, we also plan to analyze the QNMs [117–121] of various stationary spacetimes.

Appendix A. Appendices

Metric of the Reissner–Nordström BH of mass M and charge Q is given by

$$ds^2 = -\frac{\Delta}{r^2}dt^2 + \frac{r^2}{\Delta}dr^2 + r^2(d\theta^2 + \sin^2\theta d\varphi^2), \tag{A.1}$$

where $\Delta = r^2 - 2Mr + Q^2$. The locations of the event horizon and of the Cauchy horizon are $r_+ = M + \sqrt{M^2 - Q^2}$ and $r_- = M - \sqrt{M^2 - Q^2}$, respectively. To investigate the bosonic perturbation of the Reissner–Nordström BH, one should consider the scalar field Φ, which obeys the Klein–Gordon equation (2), propagating in a Reissner–Nordström BH geometry. For the chargeless case with an Ansatz $\Phi = R_0(r)Y^0_{jm}(\theta,\phi)e^{-i\omega t}$, the radial components of the fields can be found as follows [122]:

$$\frac{d}{dr}\left(\Delta\frac{dR_0}{dr}\right) + \left(\frac{K^2}{\Delta} - \lambda\right)R_s = 0, \tag{A.2}$$

where $K = \omega r^2$ and $\lambda = \ell(\ell+1)$ is a separation constant. If one makes the following transformation $f_0 = rR_0$ and adopt the tortoise coordinate r_* (defined here as $dr_*/dr = r^2/\Delta$), the radial equation (A.2) recasts in

$$\frac{d^2 f_0}{dr_*^2} + W_0(\omega, r_*)f_0 = 0, \tag{A.3}$$

where the complex function W_0 is given by

$$W_0(\omega, r_*) = \frac{\Delta}{r^4}\left[\frac{K^2}{\Delta} - 2\frac{M}{r} + 2\frac{Q^2}{r^2} - \lambda\right]. \tag{A.4}$$

By comparing Eqs. (14) and (A.3), one can easily derive the effective potential of the Reissner–Nordström BH:

$$V_0^{RN}(r) = \frac{\Delta}{r^4}\left[2\frac{M}{r} - 2\frac{Q^2}{r^2} + \lambda\right]. \tag{A.5}$$

Table 3. QNM frequencies of the Reissner–Nordström BH for the fundamental modes ($n = 0$) obtained from the continued fraction method (CFM [126]) and FNNM: Qualitative comparison of the two methods. For the sake of simplicity, in this illustrative example, we have considered the s-modes (ℓ) of the chargeless ($q = 0$) scalar fields. See [126, Table I].

Q/M	0.01	0.1	0.5	0.99	0.9999
FNNM	$0.110645 - 0.103976i$	$0.111758 - 0.104364i$	$0.115843 - 0.10628i$	$0.133596 - 0.094459i$	$0.133507 - 0.094478i$
CFM	$0.110457 - 0.104896i$	$0.110649 - 0.104938i$	$0.115764 - 0.105751i$	$0.133570 - 0.095641i$	$0.133459 - 0.095844i$

Following the Leaver's [123, 124] original continued fraction method (CFM), which was later improved by Nollert [125], with the effective potential (A.5), Richartz and Giugno [126] obtained the numerical values of the QNMs of the Reissner–Nordström BH. Comparing the numerical results of [126] with the results to be obtained from FNNM might be more meaningful and beneficial for the reader. For this purpose, we have created Table 3, which obviously shows how the two methods produce very close values.

Acknowledgments

We are thankful to the Editor and anonymous Referees for their constructive suggestions and comments.

References

[1] L. Manfredi, J. Mureika and J. Moffat, Quasinormal modes of modified gravity (MOG) black holes, *JURP* **29** (2019) 100006.
[2] P. D. Roy, S. Aneesh and S. Kar, Revisiting a family of wormholes: Geometry, matter, scalar quasinormal modes and echoes, *Eur. Phys. J. C* **80** (2020) 850.
[3] B. F. Schutz and C. M. Will, Black hole normal modes: A semianalytic approach, *Astrophys. J.* **291** (1985) L33.
[4] E. Berti, V. Cardoso and A. O. Starinets, Quasinormal modes of black holes and black branes, *Class. Quant. Grav.* **26** (2009) 163001.
[5] J. W. Guinn, C. M. Will, Y. Kojima and B. F. Schutz, High overtone normal modes of Schwarzschild black holes, *Class. Quant. Grav.* **7** (1990) L47.
[6] R. A. Konoplya and A. Zhidenko, Quasinormal modes of black holes: From astrophysics to string theory, *Rev. Mod. Phys.* **83** (2011) 793.
[7] S. Iyer, Black hole normal modes: A Wkb approach. 2. Schwarzschild black holes, *Phys. Rev. D* **35** (1987) 3632.
[8] K. H. C. Castello-Branco, R. A. Konoplya and A. Zhidenko, High overtones of Dirac perturbations of a Schwarzschild black hole and the area spectrum of quantum black holes, *Braz. J. Phys.* **35** (2005) 1149.
[9] K. H. C. Castello-Branco, R. A. Konoplya and A. Zhidenko, High overtones of Dirac perturbations of a Schwarzschild black hole, *Phys. Rev. D* **71** (2005) 047502.
[10] J. L. Jing, Dirac quasinormal modes of Schwarzschild black hole, *Phys. Rev. D* **71** (2005) 124006.
[11] J. Skakala and M. Visser, Semi-analytic results for quasi-normal frequencies, *JHEP* **1008** (2010) 061.
[12] I. Sakalli, Quasinormal modes of charged dilaton black holes and their entropy spectra, *Mod. Phys. Lett. A* **28** (2013) 1350109.
[13] I. Sakalli, Quantization of higher-dimensional linear dilaton black hole area/entropy from quasinormal modes, *Int. J. Mod. Phys. A* **26** (2011) 2263.
[14] I. Sakalli, K. Jusufi and A. Övgün, Analytical solutions in a cosmic string Born–Infeld–Dilaton black hole geometry: Quasinormal modes and quantization, *Gen. Relativity Gravitation* **50**(10) (2018) 125.
[15] A. Övgün and K. Jusufi, Quasinormal modes and greybody factors of $f(R)$ gravity minimally coupled to a cloud of strings in $2+1$ Dimensions, *Ann. Phys.* **395** (2018) 138.

[16] P. A. Gonzalez, A. Övgün, J. Saavedra and Y. Vasquez, Hawking radiation and propagation of massive charged scalar field on a three-dimensional Gödel black hole, *Gen. Relativity Gravitation* **50**(6) (2018) 62.
[17] K. Jusufi, I. Sakalli and A. Övgün, Quantum tunneling and quasinormal modes in the spacetime of the Alcubierre warp drive, *Gen. Relativity Gravitation* **50**(1) (2018) 10.
[18] A. Övgün, I. Sakalli and J. Saavedra, Quasinormal modes of a Schwarzschild black hole immersed in an electromagnetic universe, *Chin. Phys. C* **42**(10) (2018) 105102.
[19] J. Crisostomo, S. Lepe and J. Saavedra, Quasinormal modes of extremal BTZ black hole, *Class. Quant. Grav.* **21** (2004) 2801.
[20] S. Lepe and J. Saavedra, Quasinormal modes, superradiance and area spectrum for 2+1 acoustic black holes, *Phys. Lett. B* **617** (2005) 174.
[21] J. Saavedra, Quasinormal modes of Unruh's acoustic black hole, *Mod. Phys. Lett. A* **21** (2006) 1601.
[22] R. Becar, S. Lepe and J. Saavedra, Quasinormal modes and stability criterion of dilatonic black hole in 1+1 and 4+1 dimensions, *Phys. Rev. D* **75** (2007) 084021.
[23] R. Becar, S. Lepe and J. Saavedra, Decay of dirac fields in the backgrounds of dilatonic black holes, *Int. J. Mod. Phys. A* **25** (2010) 1713.
[24] E. Abdalla and D. Giugno, An extensive search for overtones in Schwarzschild black holes, *Braz. J. Phys.* **37** (2007) 450.
[25] M. Casals and A. C. Ottewill, Spectroscopy of the Schwarzschild black hole at arbitrary frequencies, *Phys. Rev. Lett.* **109** (2012) 111101.
[26] R. A. Konoplya, Massive vector field perturbations in the Schwarzschild background: Stability and unusual quasinormal spectrum, *Phys. Rev. D* **73** (2006) 024009.
[27] X. M. Kuang, J. Saavedra and A. Övgün, The effect of the Gauss–Bonnet term to Hawking radiation from arbitrary dimensional black brane, *Eur. Phys. J. C* **77**(9) (2017) 613.
[28] K. Jusufi and A. Övgün, Tunneling of massive vector particles from rotating charged black strings, *Astrophys. Space Sci.* **361**(7) (2016) 207.
[29] S. Hod, Bohr's correspondence principle and the area spectrum of quantum black holes, *Phys. Rev. Lett.* **81** (1998) 4293.
[30] L. Motl, An analytical computation of asymptotic Schwarzschild quasinormal frequencies, *Adv. Theor. Math. Phys.* **6** (2003) 1135.
[31] G. Kunstatter, *d*-dimensional black hole entropy spectrum from quasinormal modes, *Phys. Rev. Lett.* **90** (2003) 161301.
[32] N. Andersson and C. J. Howls, The asymptotic quasinormal mode spectrum of nonrotating black holes, *Class. Quant. Grav.* **21** (2004) 1623.
[33] R. A. Konoplya and C. Molina, The ringing wormholes, *Phys. Rev. D* **71** (2005) 124009.
[34] S. W. Kim, Wormhole perturbation and its quasi normal modes, *Prog. Theor. Phys. Suppl.* **172** (2008) 21.
[35] R. A. Konoplya and A. Zhidenko, Wormholes versus black holes: Quasinormal ringing at early and late times, *JCAP* **1612**(12) (2016) 043.
[36] R. Oliveira, D. M. Dantas, V. Santos and C. A. S. Almeida, Quasi-normal modes of bumblebee wormhole, *Class. Quant. Grav.* **36**(10) (2019) 105013.
[37] I. Sakalli and A. Ovgun, Tunnelling of vector particles from Lorentzian wormholes in 3+1 dimensions, *Eur. Phys. J. Plus* **130**(6) (2015) 110.
[38] I. Sakalli and A. Ovgun, Gravitinos tunneling from traversable Lorentzian wormholes, *Astrophys. Space Sci.* **359**(1) (2015) 32.

[39] A. Ovgun and M. Halilsoy, Existence of traversable wormholes in the spherical stellar systems, *Astrophys. Space Sci.* **361**(7) (2016) 214.
[40] A. Ovgun, Rotating thin-shell wormhole, *Eur. Phys. J. Plus* **131**(11) (2016) 389.
[41] K. Jusufi, A. Övgün and A. Banerjee, Light deflection by charged wormholes in Einstein–Maxwell–Dilaton theory, *Phys. Rev. D* **96**(8) (2017) 084036.
[42] M. Halilsoy, A. Ovgun and S. H. Mazharimousavi, Thin-shell wormholes from the regular Hayward black hole, *Eur. Phys. J. C* **74** (2014) 2796.
[43] K. Jusufi and A. Övgün, Gravitational Lensing by rotating wormholes, *Phys. Rev. D* **97**(2) (2018) 024042.
[44] M. G. Richarte, I. G. Salako, J. P. Morais Graca, H. Moradpour and A. Övgün, Relativistic Bose–Einstein condensates thin-shell wormholes, *Phys. Rev. D* **96**(8) (2017) 084022.
[45] A. Övgün, Light deflection by Damour–Solodukhin wormholes and Gauss–Bonnet theorem, *Phys. Rev. D* **98**(4) (2018) 044033.
[46] R. A. Konoplya, How to tell the shape of a wormhole by its quasinormal modes, *Phys. Lett. B* **784** (2018) 43; *Eur. Phys. J. C* **78**(12) (2018) 990.
[47] J. Y. Kim, C. O. Lee and M. I. Park, Quasi-normal modes of a natural AdS wormhole in Einstein–Born–Infeld gravity, *Eur. Phys. J. C* **78**(12) (2018) 990.
[48] K. A. Bronnikov, R. A. Konoplya and A. Zhidenko, Instabilities of wormholes and regular black holes supported by a phantom scalar field, *Phys. Rev. D* **86** (2012) 024028.
[49] S. Aneesh, S. Bose and S. Kar, Gravitational waves from quasinormal modes of a class of Lorentzian wormholes, *Phys. Rev. D* **97**(12) (2018) 124004.
[50] R. A. Konoplya and A. Zhidenko, Passage of radiation through wormholes of arbitrary shape, *Phys. Rev. D* **81** (2010) 124036.
[51] A. Övgün, K. Jusufi and İ. Sakallı, Exact traversable wormhole solution in bumblebee gravity, *Phys. Rev. D* **99**(2) (2019) 024042.
[52] S. H. Volkel and K. D. Kokkotas, Wormhole potentials and throats from Quasi–Normal modes, *Class. Quant. Grav.* **35**(10) (2018) 105018.
[53] A. Aragón, P. A. González, E. Papantonopoulos and Y. Vásquez, Anomalous decay rate of quasinormal modes in Schwarzschild-dS and Schwarzschild-AdS black holes, *JHEP* **2008** (2020) 120.
[54] A. Aragón, P. A. González, E. Papantonopoulos and Y. Vásquez, Quasinormal modes and their anomalous behavior for black holes in $f(R)$ gravity, arXiv:2005.11179 [gr-qc].
[55] A. Awad and G. Nashed, Generalized teleparallel cosmology and initial singularity crossing, *JCAP* **2** (2017) 046.
[56] W. El Hanafy and G. G. L. Nashed, Exact teleparallel gravity of binary black holes, *Astrophys. Space Sci.* **361**(2) (2016) 68.
[57] G. G. L. Nashed, Reissner Nordström solutions and energy in teleparallel theory, *Mod. Phys. Lett. A* **21** (2006) 2241–2250.
[58] Z. Yan, C. Wu and W. Guo, Scalar field quasinormal modes of noncommutative high dimensional Schwarzschild–Tangherlini black hole spacetime with smeared matter sources, *Nucl. Phys. B* **961** (2020) 115217.
[59] R. D. B. Fontana, P. A. González, E. Papantonopoulos and Y. Vásquez, Anomalous decay rate of quasinormal modes in Reissner–Nordström black holes, *Phys. Rev. D* **103**(6) (2021) 064005.
[60] G. Panotopoulos and Á. Rincón, Quasinormal spectra of scale-dependent Schwarzschild–de Sitter black holes, *Phys. Dark Univ.* **31** (2021) 100743.

[61] P. Mourier, X. Jiménez Forteza, D. Pook-Kolb, B. Krishnan and E. Schnetter, Quasinormal modes and their overtones at the common horizon in a binary black hole merger, *Phys. Rev. D* **103**(4) (2021) 044054.
[62] J. C. Fabris, M. G. Richarte and A. Saa, Quasinormal modes and self-adjoint extensions of the Schrödinger operator, *Phys. Rev. D* **103**(4) (2021) 045001.
[63] M. Villani, Quasi-normal mode of a regular Schwarzschild black hole, *Class. Quant. Grav.* **37**(21) (2020) 215019.
[64] C. Y. Chen, Y. H. Kung and P. Chen, Black hole perturbations and quasinormal modes in hybrid Metric-Palatini Gravity, *Phys. Rev. D* **102**(12) (2020) 124033.
[65] P. Burikham, S. Ponglertsakul and T. Wuthicharn, Quasi-normal modes of near-extremal black holes in generalized spherically symmetric spacetime and strong cosmic censorship conjecture, *Eur. Phys. J. C* **80**(10) (2020) 954.
[66] J. Matyjasek, Quasinormal modes of dirty black holes in the effective theory of gravity with a third order curvature term, *Phys. Rev. D* **102**(12) (2020) 124046.
[67] A. Aragón, R. Bécar, P. A. González and Y. Vásquez, Massive Dirac quasinormal modes in Schwarzschild–de Sitter black holes: Anomalous decay rate and fine structure, *Phys. Rev. D* **103**(6) (2021) 064006.
[68] E. Witten, Anti-de Sitter space and holography, *Adv. Theor. Math. Phys.* **2** (1998) 253.
[69] G. T. Horowitz and V. E. Hubeny, Quasinormal modes of AdS black holes and the approach to thermal equilibrium, *Phys. Rev. D* **62** (2000) 024027.
[70] B. Wang, C. Molina and E. Abdalla, Evolving of a massless scalar field in Reissner–Nordstrom Anti-de Sitter space-times, *Phys. Rev. D* **63** (2001) 084001.
[71] V. Cardoso and J. P. S. Lemos, Scalar, electromagnetic and Weyl perturbations of BTZ black holes: Quasinormal modes, *Phys. Rev. D* **63** (2001) 124015.
[72] E. Berti and K. D. Kokkotas, Quasinormal modes of Reissner–Nordstrom–anti-de Sitter black holes: Scalar, electromagnetic and gravitational perturbations, *Phys. Rev. D* **67** (2003) 064020.
[73] B. Wang, E. Abdalla and R. B. Mann, Scalar wave propagation in topological black hole backgrounds, *Phys. Rev. D* **65** (2002) 084006.
[74] S. Musiri and G. Siopsis, Asymptotic form of quasinormal modes of large AdS black holes, *Phys. Lett. B* **576** (2003) 309.
[75] T. R. Govindarajan and V. Suneeta, Quasinormal modes of AdS black holes: A Superpotential approach, *Class. Quant. Grav.* **18** (2001) 265.
[76] E. Abdalla, K. H. C. Castello-Branco and A. Lima-Santos, Support of dS/CFT correspondence from space-time perturbations, *Phys. Rev. D* **66** (2002) 104018.
[77] C. Chirenti and M. G. Rodrigues, Effect of a variable cosmological constant on black hole quasinormal modes, *Phys. Rev. D* **92**(8) (2015) 084051.
[78] D. P. Du, B. Wang and R. K. Su, Quasinormal modes in pure de Sitter space-times, *Phys. Rev. D* **70** (2004) 064024.
[79] L. M. Burko and G. Khanna, Late-time Kerr tails revisited, *Class. Quant. Grav.* **26** (2009) 015014.
[80] K. Destounis, R. D. Fontana and F. C. Mena, Accelerating black holes: Quasinormal modes and late-time tails, *Phys. Rev. D* **102**(4) (2020) 044005.
[81] M. L. Piscopo, M. Spannowsky and P. Waite, Solving differential equations with neural networks: Applications to the calculation of cosmological phase transitions, *Phys. Rev. D* **100** (2019) 016002.
[82] P. Tahmasebi and A. Hezarkhani, A Application of a modular feedforward neural network for grade estimation, *Nat. Resour. Res.* **20** (2011) 25–32.

[83] A. Menéndez-Vázquez, M. Kolstein, M. Martínez and L. M. Mir, Searches for compact binary coalescence events using neural networks in the LIGO/Virgo second observation period, *Phys. Rev. D* **103**(6) (2021) 062004.
[84] C. Dreissigacker and R. Prix, Deep-learning continuous gravitational waves: Multiple detectors and realistic noise, *Phys. Rev. D* **102**(2) (2020) 022005.
[85] G. J. Wang, X. J. Ma and J. Q. Xia, Machine learning the cosmic curvature in a model-independent way, *Mon. Not. Roy. Astron. Soc.* **501**(4) (2021) 5714–5722.
[86] G. Vajente, Y. Huang, M. Isi, J. C. Driggers, J. S. Kissel, M. J. Szczepanczyk and S. Vitale, Machine-learning nonstationary noise out of gravitational-wave detectors, *Phys. Rev. D* **101**(4) (2020) 042003.
[87] R. Ciuca and O. F. Hernández, Inferring cosmic string tension through the neural network prediction of string locations in CMB maps, *Mon. Not. Roy. Astron. Soc.* **483**(4) (2019) 5179–5187.
[88] S. Khan and R. Green, Gravitational-wave surrogate models powered by artificial neural networks, *Phys. Rev. D* **103**(6) (2021) 064015.
[89] S. R. Green and J. Gair, Complete parameter inference for GW150914 using deep learning, arXiv:2008.03312 [astro-ph.IM].
[90] G. R. Santos, M. P. Figueiredo, A. d. Santos, P. Protopapas and T. A. E. Ferreira, Gravitational wave detection and information extraction via neural networks, arXiv:2003.09995 [gr-qc].
[91] L. Haegel and S. Husa, Predicting the properties of black-hole merger remnants with deep neural networks, *Class. Quant. Grav.* **37**(13) (2020) 135005.
[92] C. Dreissigacker, R. Sharma, C. Messenger, R. Zhao and R. Prix, Deep-learning continuous gravitational waves, *Phys. Rev. D* **100**(4) (2019) 044009.
[93] D. George and E. A. Huerta, Deep learning for real-time gravitational wave detection and parameter estimation: Results with advanced LIGO data, *Phys. Lett. B* **778** (2018) 64–70.
[94] H. Gabbard, M. Williams, F. Hayes and C. Messenger, Matching matched filtering with deep networks for gravitational-wave astronomy, *Phys. Rev. Lett.* **120**(14) (2018) 141103.
[95] D. R. Parisi, M. C. Mariani and M. A. Laborde, Solving differential equations with unsupervised neural networks, *Chem. Eng. Process.* **42** (2003) 715–721.
[96] N. Yadav, A. Yadav and M. Kumar, *An Introduction to Neural Network Methods for Differential Equations* (Springer, New York, 2015).
[97] H. Mutuk, Cornell potential: A neural network approach, *Adv. High Energy Phys.* **2019** (2019) 3105373.
[98] H. Mutuk, Mass spectrum of exotic $X(5568)$ state via artificial neural network, *Int. J. Mod. Phys. A* **34**(28) (2019) 1950167.
[99] H. Nakano *et al.*, Comparison of various methods to extract ringdown frequency from gravitational wave data, *Phys. Rev. D* **99**(12) (2019) 124032.
[100] Y. B. Kim, C. Y. Oh and N. Park, Classical geometry of de Sitter space-time: An introductory review, arXiv:hep-th/0212326.
[101] T. R. Govindarajan and V. Suneeta, Quasinormal modes of AdS black holes: A Superpotential approach, *Class. Quant. Grav.* **18** (2001) 265.
[102] A. Chella, A. Gentile, F. Sorbello and A. Tarantino, Supervised learning for feedforward neural networks: A new minimax approach for fast convergence, in *IEEE International Conference on Neural Networks*, Vol. 1, San Francisco, CA, USA (1993), pp. 605–609.
[103] D. Guidici and M. Clark, One-dimensional convolutional neural network land-cover classification of multi-seasonal hyperspectral imagery in the San Francisco Bay Area, California, *Remote Sens.* **9** (2017) 629.

[104] S. Hod, Quasinormal resonances of near-extremal Kerr–Newman black holes, *Phys. Lett. B* **666** (2008) 483.
[105] L. Detweiler, *Sources of Gravitational Radiation* (Cambridge Univ. Press, Cambridge, 1979).
[106] A. Rostworowski, Quasinormal frequencies of D-dimensional Schwarzschild black holes: Evaluation via continued fraction method, *Acta Phys. Polon. B* **38** (2007) 81.
[107] S. Chakraverty and S. Mall, *Artificial Neural Networks for Engineers and Scientists-Solving Ordinary Differential Equations* (CRC Press, Boca Raton, FL, 2017).
[108] H. Mutuk, Neural network study of hidden-charm pentaquark resonances, *Chin. Phys. C* **43**(9) (2019) 093103.
[109] I. E. Lagaris, A. Likas and D. I. Fotiadis, Artificial neural network methods in quantum mechanics, *Comput. Phys. Commun.* **104** (1997) 1.
[110] A. Liaqat, M. Fukuhara and T. Takeda, Application of neural network collocation method to data assimilation, *Comput. Phys. Comm.* **141** (2001) 350.
[111] J. R. Noriega and H. Wang, A direct adaptive neural-network control for unknown nonlinear systems and its application, *IEEE Trans. Neural Netw.* **9** (1998) 27.
[112] A. V. Pavlov, J. A. Serdyuk and A. B. Ustinov, Machine learning and the Schrodinger equation, *J. Phys.: Conf. Ser.* **1236** (2019) 12050.
[113] D. Pfau, J. S. Spencer, A. G. de G. Matthews and W. M. C. Foulkes, Ab-initio solution of the many-electron schrodinger equation with deep neural networks, *Phys. Rev. Res.* **2** (2020) 033429.
[114] E. Newman and R. Penrose, An approach to gravitational radiation by a method of spin coefficients, *J. Math. Phys.* **3** (1962) 566.
[115] S. Chandrasekhar, *The Mathematical Theory of Black Holes* (Oxford University Press, Oxford, 1983).
[116] I. Sakalli and M. Halilsoy, Solution of dirac equation in the near horizon geometry of an extreme Kerr black hole, *Phys. Rev. D* **69** (2004) 124012.
[117] J. D. Bekenstein, The quantum mass spectrum of the Kerr black hole, *Lett. Nuovo Cim.* **11** (1974) 467.
[118] J. D. Bekenstein, Quantum black holes as atoms, arXiv:gr-qc/9710076.
[119] J. D. Bekenstein, Black holes: Classical properties, thermodynamics and heuristic quantization, arXiv:gr-qc/9808028.
[120] I. Sakalli, Quantization of rotating linear dilaton black holes, *Eur. Phys. J. C* **75**(4) (2015) 144.
[121] I. Sakalli and G. Tokgoz, Spectroscopy of rotating linear dilaton black holes from boxed quasinormal modes, *Annalen Phys.* **528** (2016) 612.
[122] J. Jing, Q. Y. Pan and X. He, Resonant frequencies of charged scalar and Dirac fields in Kerr–Newman black-hole space-time, *Int. J. Mod. Phys. D* **16** (2007) 81–92.
[123] E. W. Leaver, An analytic representation for the quasi normal modes of Kerr black holes, *Proc. Roy. Soc. Lond. A* **402** (1985) 285–298.
[124] E. W. Leaver, Quasinormal modes of Reissner–Nordstrom black holes, *Phys. Rev. D* **41** (1990) 2986–2997.
[125] H. P. Nollert, Quasinormal modes of Schwarzschild black holes: The determination of quasinormal frequencies with very large imaginary parts, *Phys. Rev. D* **47** (1993) 5253–5258.
[126] M. Richartz and D. Giugno, Quasinormal modes of charged fields around a Reissner–Nordström black hole, *Phys. Rev. D* **90**(12) (2014) 124011.